Mixing and noise in diffusion and phonon cooled superconducting hot-electron bolometers

P. J. Burke,[a] R. J. Schoelkopf, and D. E. Prober
Departments of Applied Physics and Physics, Yale University, 15 Prospect Street, New Haven, Connecticut 06520-8284

A. Skalare, B. S. Karasik, M. C. Gaidis, W. R. McGrath, B. Bumble, and H. G. LeDuc
Center for Space Microelectronics Technology, Jet Propulsion Laboratory, Caltech, Pasadena, California 91109

(Received 27 July 1998; accepted for publication 19 October 1998)

We report a systematic, comprehensive set of measurements on the dynamics and noise processes in diffusion and phonon-cooled superconducting hot-electron bolometer mixers which will serve as ultralow noise detectors in THz heterodyne receivers. The conversion efficiency and output noise of devices of varying lengths were measured with radio frequency between 8 and 40 GHz. The devices studied consist of 100-Å-thin film Nb bridges connected to thick (1000 Å), high conductivity normal metal (Au) leads. The lengths of the devices studied range from 0.08 to 3 μm. For devices longer than the electron–phonon interaction length $L_{e-ph} \equiv \sqrt{D\tau_{e-ph}}$, with D the diffusion constant and τ_{e-ph}^{-1} the electron–phonon interaction rate, the hot electrons are cooled dominantly by the electron–phonon interaction, which in Nb is too slow for practical applications. If the device length is less than πL_{e-ph} (≈ 1 μm at 4.2 K), then out diffusion of heat into the high conductivity leads dominates the cooling process. In this limit, the intermediate frequency (IF) bandwidth is found to vary as L^{-2}, with L the bridge length, as expected for diffusion cooling. The shortest device has an IF bandwidth greater than 6 GHz, the largest reported for a low-T_c superconducting bolometric mixer. The dominant component of the output noise decreases with frequency in the same manner as the conversion efficiency, consistent with a model based on thermal fluctuations. The noise bandwidth is larger than the gain bandwidth, and the mixer noise is *low*, ranging from 100 to 530 K (double sideband). The crossover from phonon dominated to diffusion dominated behavior is also demonstrated using noise thermometry measurements in the normal state. Scalar measurements of the device differential impedance in the intermediate state agree with a theoretical model which takes into account the thermal and electrical dynamics. We also present detailed comparisons with theoretical predictions of the output noise and conversion efficiency. © *1999 American Institute of Physics.* [S0021-8979(99)08602-8]

I. INTRODUCTION

Recent research on hot-electron bolometer (HEB) mixers has enhanced the prospect of achieving quantum-noise-limited performance ($T_Q = h\nu/k$) in heterodyne receivers at THz frequencies. Hot-electron bolometer mixers of both the phonon cooled[1] and diffusion cooled[2–4] type have already shown excellent noise performance. To date, the lowest noise receivers in the submillimeter band use as detectors superconducting-insulating-superconducting (SIS) tunnel junctions.[5,6] Nb SIS mixers have degraded performance above the energy gap frequency, $\approx$700 GHz, and are expected to sharply degrade above twice this frequency. Schottky diodes are used at frequencies above 1 THz, but are much noisier (typically no better than 150 times the quantum limit) and require large local oscillator (LO) power, of order mW. Hot-electron bolometric mixers using the heating-induced nonlinearity in a superconductor near T_c can achieve low noise and reasonable conversion efficiency. Such devices are attractive because they have no parasitic capacitance, simplifying the radio frequency (rf) coupling, and require small LO power, $\approx$10 nW. Bolometric mixers are expected to perform well in the THz frequency range, without limits related to the energy gap frequency, since they rely only on heating of the electrons in the device.

In hot-electron bolometers, the electrons are heated by direct current (dc) and rf power above the temperature of the lattice. For slow variations of power, the temperature shift is proportional to the power absorbed. Thus,

$$\delta T \sim P = V(t)^2/R \sim (V_{LO}\cos(\omega_{LO}t) + V_{sig}\cos(\omega_{sig}t))^2$$
$$\sim V_{LO}V_{sig}\cos[(\omega_{LO} - \omega_{sig})t] + \text{dc term}. \quad (1)$$

Here δT is the temperature change, $V(t)$ the net time dependent voltage, R the device resistance, V_{LO} and V_{sig} the LO and signal voltages, respectively, and ω_{LO} and ω_{sig} the LO and signal frequencies, respectively. Since the temperature changes at the intermediate frequency (IF $= \omega_{LO} - \omega_{sig}$), the resistance changes at the IF, thus leading to an oscillating voltage at the IF under a current bias. An important constraint is that the IF must be less than the energy-relaxation

[a]Current address: MS114-36 Condensed Matter Physics, Caltech, Pasadena, California 91125; electronic mail: pjburke@cco.caltech.edu

rate for the electron system, otherwise the electron temperature will be unable to follow power variation at the IF. It is this issue that has limited the use of hot-electron-bolometer mixers, and which research in this article addresses in a very direct way.

The hot-electron effect in Nb was first studied in the early 1980's,[7–14] with the first official proposal and analysis for the use of the hot-electron-bolometer as a mixer appearing in Ref. 14. In these experiments, it was found that the electron–phonon interaction time was ≈ 1 ns at 4.2 K for dirty films (with a diffusion constant of $D=1$ cm^2/s). This would allow for an IF 3 dB gain bandwidth, defined as the IF at which the conversion efficiency drops by 3 dB, of ≈ 150 MHz, which is still too small for practical applications. Additional theoretical modeling[14] suggested that the mixer noise temperature $T_{\rm mix}$, the noise referred to the device input, could approach 50 K, which is the quantum limit at 1 THz. This prediction was independent of the rf frequency, as long as the rf radiation was absorbed by the electron system. Thus, the noise was predicted to be low up to very high rf frequencies. However, the IF bandwidth was not sufficient.

Two approaches have been proposed to increase the intermediate frequency bandwidth of the superconducting bolometer, while keeping the noise low and the rf range broad. The first approach is to use a material with a shorter electron–phonon interaction time. NbN has a somewhat higher T_c than Nb, and a much stronger electron–phonon interaction. The predicted noise is still low, and the rf frequency range should also be broad. Initial experiments indicated an IF bandwidth of 5.3 GHz.[15,16] There, results between 1.6 and 5.3 K were presented. By extrapolating the data to 10 K, the authors predicted a bandwidth of 10 GHz could be achieved. Subsequent experiments have been unable to reproduce these results. The results have varied for the IF bandwidth (0.6,[17] 1.1,[18] 0.8,[19,20] 3–4,[21] 1.6,[22] and 2.2 GHz[1]). For some films comparable to those of Ref. 16, the mixing bandwidth was less than 1 GHz. Recent experiments[23,24] indicate that control of the film thickness may allow more control over the achieved bandwidth for NbN. Very thin films (3.5 nm) achieve the largest bandwidths. Promising receiver noise temperatures have also been achieved, between 410 K double sideband (DSB) at an rf frequency of 410 GHz,[1] and 9000 K DSB at 1.2 THz.[21] Thus NbN is worthy of further investigation.

A different approach was proposed by one of us in Ref. 25, and is investigated in this article. The approach consists of using a very short strip of Nb of length L as the hot-electron bolometer, with L less than the electron–phonon interaction length, $L_{\rm e-ph}\equiv\sqrt{D\tau_{\rm e-ph}}$, where $\tau_{\rm e-ph}^{-1}$ is the electron–phonon interaction rate and D the diffusion constant. For short devices, very fast cooling of the electrons can occur by out diffusion of heat into high-conductivity, normal metal leads. In this case, the effective thermal time constant is related to the diffusion time, and is given by

$$\tau_{\rm th}=\frac{L^2}{\pi^2 D}. \tag{2}$$

Thus, for a 0.1μm bridge with a diffusion constant of 1 cm^2/s, a time constant of order 10 ps is predicted, allowing an IF bandwidth of order 10 GHz to be achieved. To date, excellent receiver noise results based on diffusion-cooled HEBs have been obtained by some of us at rf frequencies of 0.5 (650 K DSB),[2] 1.2 (1880 K DSB),[3] and 2.5 THz (2750 K DSB).[4] Other groups have achieved similar results for receiver noise temperatures using diffusion-cooled HEBs, namely 2200 K DSB at 730 GHz[26] and 1500 K DSB at 660 GHz.[27]

The experiments described in this article were designed not to produce practical receivers but to systematically test device performance as a function of device length under a variety of operating conditions. We present measurements of the spectrum of the output noise, conversion efficiency, and mixer noise for phonon and diffusion cooled Nb devices of various thermal time constants, and compare these results to theoretical predictions. (Some of the results have been published in Refs. 28 and 29.) The devices vary in length from 0.08 ($<L_{\rm eph}$) to 3 μm ($>L_{\rm eph}$). Additionally, we present measurements of the device differential impedance over a very broadband (0.1–7.5 GHz). Finally, we present noise thermometry measurements of the device in the normal state which demonstrate the crossover from phonon to diffusion cooling in a clear way. Since the mixing process is thermal, these measurements are expected to be representative of, and provide design guidance for, devices used in future THz heterodyne receivers. We compare below to THz measurements.

II. THEORY

For a lumped thermal element, theoretical calculations based purely on thermodynamics have already been performed which relate the device conversion efficiency and output noise to the dc current, LO power, device resistance, thermal conductance, temperature, and change of resistance with temperature (dR/dT).[30–33] These are summarized below. The results of our calculations for the distributed system are given later in this section and related to the lumped element approach calculations already available in the literature.

A. Lumped element predictions

1. Conversion efficiency

The coupled conversion efficiency, defined as the power out at the IF over the power in at the rf, can be predicted in terms of the dc current $I_{\rm dc}$, the LO power $P_{\rm LO}$, the thermal conductance to the bath G, the resistance $R\equiv V_{\rm dc}/I_{\rm dc}$, and the change in resistance with temperature dR/dT as[30–33]

$$\eta(\omega)=\eta_{\rm IF}\frac{P_{\rm LO}}{2R}\left(\frac{I_{\rm dc}(dR/dT)}{G_{\rm eff}}\right)^2\frac{1}{1+(\omega\tau_{\rm eff})^2} \tag{3}$$

$$=\eta(0)\frac{1}{1+(\omega\tau_{\rm eff})^2}, \tag{4}$$

where ω is the IF. This is the single-sideband (SSB) efficiency. We define the ''gain bandwidth'' as the IF at which the conversion efficiency drops to 3 dB relative to its low IF value. Thus, from Eq. (3), the gain bandwidth is given by

$f_{3\ \mathrm{dB,gain}}=1/(2\pi\tau_{\mathrm{eff}})$. Here τ_{eff} is the effective thermal time constant and G_{eff} the effective thermal conductance to the bath. The effective thermal conductance and time constant are related to the ''bare'' thermal conductance G and time constant τ_{th} by

$$\tau_{\mathrm{eff}}\equiv\tau_{\mathrm{th}}/(1-\alpha), \tag{5}$$

$$\tau_{\mathrm{th}}\equiv C/G, \tag{6}$$

$$G_{\mathrm{eff}}\equiv G(1-\alpha), \tag{7}$$

$$\alpha\equiv\frac{I_{\mathrm{dc}}^2 dR/dT}{G}\left(\frac{R_L-R}{R_L+R}\right), \tag{8}$$

$$=\alpha_0\left(\frac{R_L-R}{R_L+R}\right), \tag{9}$$

$$\alpha_0\equiv\frac{I_{\mathrm{dc}}^2 dR/dT}{G}, \tag{10}$$

where C is the (electronic) heat capacity, and R_L the load resistance at the IF, i.e., the input resistance of the IF amplifier, which is typically $50\,\Omega$. The effect of the electrothermal feedback between the electron temperature and the dc bias supply is described quantitatively by the parameter α. If α is small (due to small current or small dR/dT), then the effect of electrothermal feedback is small, and the effective time constant τ_{eff} is equal to the ''bare'' thermal time constant τ_{th}, and the effective thermal conductance G_{eff} is equal to the bare thermal conductance G. The IF load resistance tends to suppress electrothermal feedback if the device resistance R is comparable to the load resistance R_L. This is the case for the devices studied in this work.

The factor η_{IF} is defined as

$$\eta_{\mathrm{IF}}\equiv\frac{4RR_L}{(R+R_L)^2}, \tag{11}$$

where R_L is the IF load resistance. This factor is not a standard mismatch factor in the usual sense, since the device impedance depends on frequency, whereas Eq. (11) is independent of frequency. The factor results from a more rigorous calculation of the effect of a finite load impedance at the IF on the electron dynamics.[30,32,33] The parameter varies between zero and one, and is one when the device resistance is equal to the input impedance of the IF amplifier.

2. Output noise

In hot-electron bolometers, the important noise sources are expected to be thermal fluctuation noise and Johnson noise. Thermodynamic fluctuations in the electron temperature cause resistance fluctuations and hence voltage fluctuations under current bias. The prediction for the output noise due to thermal fluctuations T_{TF} is given by[30–33]

$$T_{\mathrm{TF}}(\omega)=(I_{\mathrm{dc}}T_e(dR/dT))^2\frac{1}{RG_{\mathrm{eff}}(1-\alpha)}\frac{1}{1+(\omega\tau_{\mathrm{eff}})^2}\eta_{\mathrm{IF}} \tag{12}$$

$$=T_{\mathrm{TF}}(0)\frac{1}{1+(\omega\tau_{\mathrm{eff}})^2}, \tag{13}$$

where η_{IF} is the IF mismatch factor in Eq. (11), and T_e the electron temperature. The Johnson noise will be equal to the temperature of the electrons. There is a small correction to the Johnson noise due to electrothermal feedback,[32–34] which can be neglected in the experiments presented here.

B. Distributed system predictions

For a distributed nonsuperconducting system, the output noise temperature due to Johnson noise is predicted to be the average temperature along the length of the bridge. However, a quantitative theory for the conversion efficiency and thermal fluctuation noise which treats the device as a distributed system has not yet been developed.[35] We therefore define an effective thermal conductance as the average electron temperature rise over the length of the device divided by the input power. We have calculated this quantity in the absence of electron phonon interactions[25,36] when the dissipation of power is spatially uniform. We find

$$G=\frac{\mathcal{L}T_b}{R/12}. \tag{14}$$

We also find an effective thermal time constant is given to a good approximation by

$$\tau_{\mathrm{th}}=\frac{L^2}{\pi^2 D}. \tag{15}$$

These results are true in the limit that the device length is less than $L_{\mathrm{e-ph}}$. Since a full theory for a distributed bolometer has not yet been developed, we use the lumped element predictions with an effective thermal conductance given by Eq. (14) and an effective time constant given by Eq. (15). For devices much longer than $L_{\mathrm{e-ph}}$, the relevant quantities to use are $G_{\mathrm{e-ph}}$, the electron–phonon thermal conductance, and $\tau_{\mathrm{e-ph}}$. In the intermediate range, the cooling rates due to diffusion and the electron-phonon interaction should approximately add, and this approximation will be used in the remainder of this article.

It is possible that the dissipation of power is not uniform along the length of the device. The impedance of the device at frequencies above the energy gap frequency ($\approx$700 GHz in bulk Nb) is constant and equal to the normal state impedance. Therefore, if a high frequency signal is applied above the energy gap frequency, then the dissipation of power is uniform. However, if the frequency of the applied signal is less than the energy gap frequency, then it is possible that the dissipation of power varies spatially, since the temperature and hence resistance vary spatially. At T_c the energy gap vanishes, suggesting that the dissipation of power may still be uniform at all frequencies.

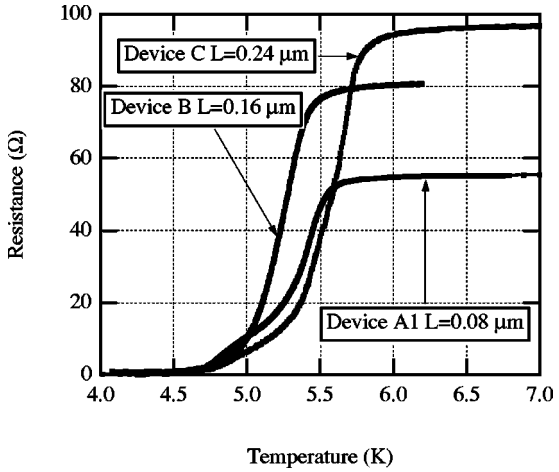

FIG. 1. Resistance vs. temperature curves for diffusion-cooled devices.

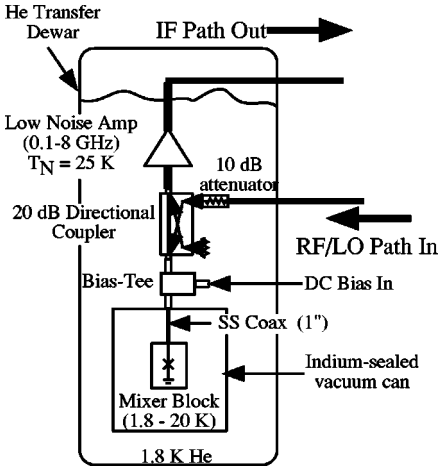

FIG. 2. Schematic of experimental setup.

III. EXPERIMENTAL TECHNIQUE

A. Device fabrication

The devices studied were all fabricated from the same thin (100 Å) Nb film, deposited on a quartz substrate. The patterned film has a transition temperature of $T_c \approx 5$ K, transition width $\Delta T_c \sim 0.5$ K, and sheet resistance $\approx 29\,\Omega$. The length of the bridge was defined by the normal metal (1000-Å-thick Au) contacts using direct write e-beam lithography in a self-aligned process.[37] The length and width of the devices measured in this work were determined by inspecting the scanning electron microscopy (SEM) image of different devices with the same design length in the same fabrication run. The estimated error using this technique is approximately $\pm 0.05\,\mu$m. The devices measured in this work were not measured in an SEM, in order to avoid electrical damage. The measured resistance versus temperature curves are plotted in Fig. 1.

B. Measurement technique and calibrations

Each device was mounted at the end of a section of 50 Ω microstrip, using a ''flip-chip'' configuration to assure a broadband match. A cooled directional coupler was used to weakly couple in the rf and LO. The through port was connected to a cooled, low noise ($\approx$25K), broadband amplifier. The cable losses, amplifier gain, and coupler performance were each measured at 2 K. The mixer conversion efficiency as a function of intermediate frequency was thus measured to ± 2 dB. The amplifier chain noise and gain were calibrated *in situ* to the plane of the device by heating the device above T_c and using it as a variable temperature load. This calibration applies for a source impedance given by R_n. Some measurements were performed with an isolator to confirm that impedance mismatch effects were not significantly affecting the calibration. Additional measurements of the return loss of the devices were performed in order to determine the impedance mismatch in the intermediate state. The power coupling was 90% or better over the frequency range measured for all the devices, except device *E*. Therefore, the lack of an isolator should not significantly modify the calibration constants of the amplifier gain and noise which were determined when the device was in the normal state. A schematic of the experimental setup is shown in Fig. 2.

IV. EXPERIMENTAL RESULTS

A. Conversion efficiency and noise

The measured conversion efficiency, output noise, and mixer noise all depend on several parameters under experimental control for a given device. We first discuss the dependence on LO power, then on dc power, then on the IF. The measurements of the conversion efficiency and noise were all performed at a bath temperature of 2 K.

1. Conversion efficiency and noise vs LO power

The (relative) conversion efficiency, output noise, and mixer noise are plotted as a function of LO power for fixed dc voltage in Fig. 3 for device A1. There are two cases of LO power which are of interest. We refer to the LO power required to maximize the (coupled) conversion efficiency as the ''optimum efficiency'' case. (This occurs at 0 dB in Fig. 3.) Note that the conversion efficiency and output noise peak

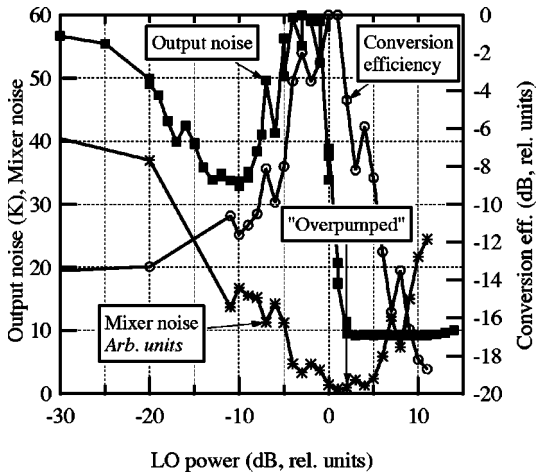

FIG. 3. Efficiency, output noise, and mixer noise vs LO power for device A1.

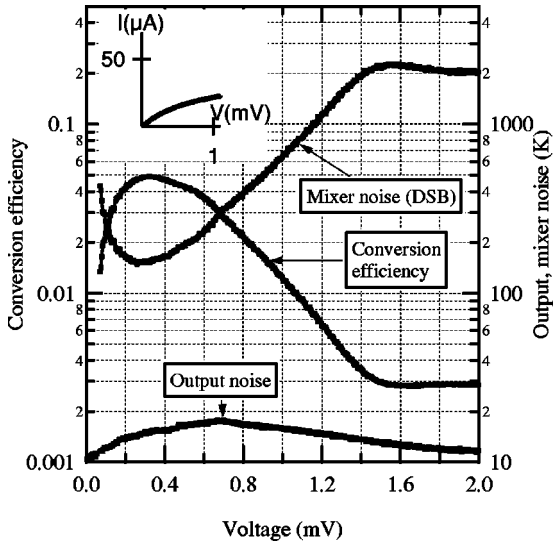

FIG. 4. Efficiency, output noise, and mixer noise vs voltage for device B in overpumped case. IF=125–215 MHz.

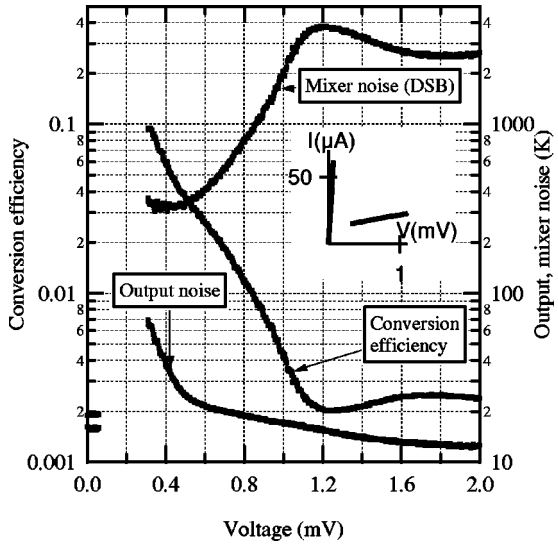

FIG. 5. Efficiency, output noise, and mixer noise vs voltage for device B in optimum efficiency case. IF=125–215 MHz.

at different LO powers, for a fixed bias voltage. However, the *mixer* noise is relatively constant near its minimum, even though the efficiency and output noise are changing very rapidly with LO power there. The second qualitative case is the ''overpumped'' case, where the critical current is suppressed. In that case, the output noise is drastically suppressed relative to its maximum value. The conversion efficiency is also somewhat lower than its maximum value. However, the mixer noise does not change much between the optimum efficiency case and the overpumped case. The overpumped case is of practical interest because the output noise and efficiency are less sensitive to the dc bias voltage, which will be discussed next. The general behavior indicated in Fig. 3 was observed in all the devices measured. For all the devices measured, the *mixer* noise in the overpumped case at the dc bias that minimized the mixer noise was lower than the mixer noise in the optimum efficiency case at the dc bias that minimized the mixer noise.

The output noise and conversion efficiency vary continuously with LO and dc power. This is consistent with the thermodynamic theory, since the electron temperature, thermal conductance, and dR/dT will all change with LO and dc power. We present data in the optimum efficiency and overpumped cases since they are the most interesting from an applied point of view. We do not have any evidence that there is any difference in the microscopic states of the bolometer in the two cases, since we only measure the average property of the entire device. The current–voltage *(I–V)* curves for the overpumped and optimum efficiency cases are shown in the insets of Figs. 4 and 5, respectively.

2. Conversion efficiency and noise vs dc power

In order to investigate the dependence of the conversion efficiency and noise on dc bias, the output noise and conversion efficiency were measured as a function of dc bias for two different LO powers (optimum efficiency and overpumped) for each device. The resultant mixer noise was calculated by taking the ratio of the output noise to the conversion efficiency. The measurements were done at an IF that is low enough to be representative of the zero IF limit of the device performance. The results for a typical device (device B) are plotted in Figs. 4 and 5. The immediate conclusion in these graphs is that the mixer noise is *very low*, $\approx$200 to 300 K (DSB). In the overpumped case, the conversion efficiency, output noise, and mixer noise are seen to depend smoothly on the dc bias.

3. Conversion efficiency vs intermediate frequency

One of the most important goals of this work is to investigate the dependence of the conversion efficiency on the IF and determine the time constant as a function of device length. The dependence of the relative conversion efficiency on IF is plotted for all the devices measured in Fig. 6. A

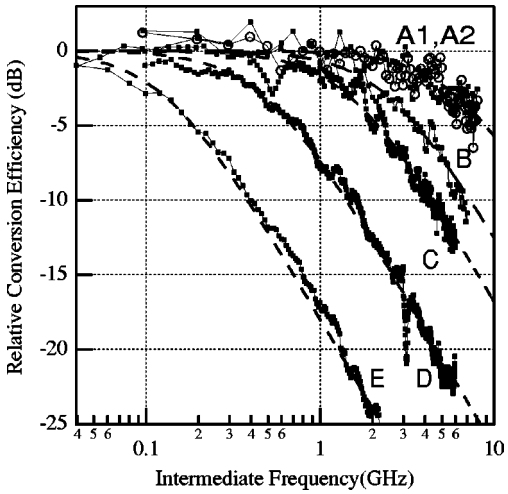

FIG. 6. Relative efficiency vs intermediate frequency for all devices. Note the excellent agreement between devices A1, A2. The dashed lines are theoretical fits to Eq. (4), where a two parameter fit to the data has been performed. The two parameters varied are τ_{eff} and $\eta(0)$. (For devices D and E, the optimum efficiency case is plotted. For the other devices, the overpumped case is plotted.)

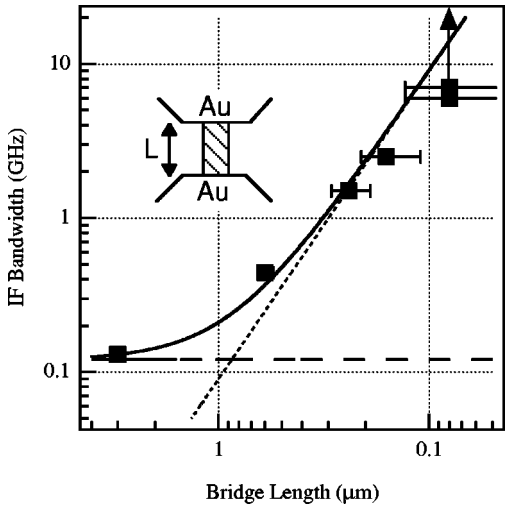

FIG. 7. Scaling of bandwidth with length. The errors on the device length are $\pm 0.05\ \mu$m. The measured bandwidth on devices A1 and A2 are lower limits, indicated by the arrow. (For devices D and E, the optimum efficiency case is plotted. For the other devices, the overpumped case is plotted.)

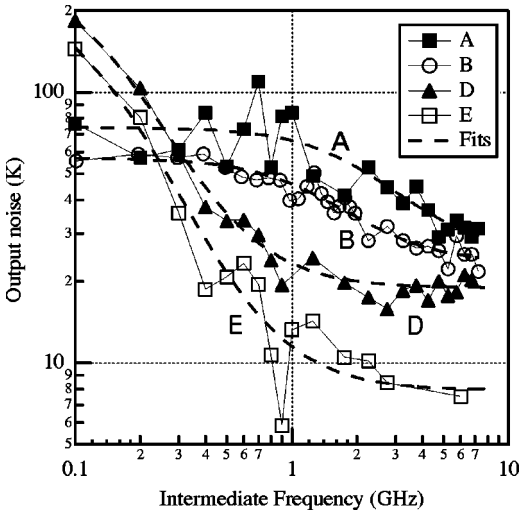

FIG. 8. Output noise vs intermediate frequency, optimum efficiency case. The dashed lines are theoretical predictions of Eq. (16), where a three-parameter fit of Eq. (16) to the data has been performed. The three parameters varied are $T_{\mathrm{TF}}(0)$, T_J, and τ_{eff}.

two-parameter fit to Eq. (4) was performed; $\eta(0)$ and τ_{eff} were varied. The theoretical fits to the data are also shown. The frequency dependence of the conversion efficiency is indeed well described by Eq. (4). Note that there are two devices of the shortest length plotted (A1,A2), and the data are very consistent. The close agreement between the theory and experiment provides strong confirmation of the theoretical model over two orders of magnitude in frequency and conversion efficiency.

The fitted time constant is plotted in Fig. 7 as a function of length. This plot is the central result of this article. When the device length L is much larger than $\pi L_{\mathrm{e-ph}}(\approx 1\ \mu\mathrm{m}$ at 4.2 K), the bandwidth is expected to be independent of length. The dashed line indicates this phonon cooling limit. Device E is in this limit. For $L \ll \pi L_{\mathrm{e-ph}}$, the dominant cooling mechanism should be diffusion, and the dotted line shows the expected L^{-2} dependence. The solid line shows the prediction for the net effect of both phonon and diffusion cooling mechanisms, assuming the thermal cooling rates add. The theoretical prediction for the diffusion cooling based on Eq. (15) is that $\tau_{\mathrm{th}}(ns) \approx 1.0\ L^2$, with L in μm. We find experimentally that $\tau_{\mathrm{th}}(ns) \approx 1.8\ L^2$. This discrepancy appears to be within the uncertainties in the predicted as well as the measured prefactor. The measured bandwidth of 6 GHz is the largest bandwidth yet obtained in a low-T_c bolometric mixer. The value of 6 GHz is actually a lower limit, since the conversion efficiency changes with IF by an amount comparable to the experimental uncertainties for the IF frequencies used.

It is possible that the measured time constant (τ_{eff}) is modified by electrothermal feedback effects, and that the bare time constant is different from the measured one. However, in Sec. IV D, the ''slowing factor'' (α) is estimated, and for all the devices it is less than 0.25, with the exception of device E. For device E, α is 0.46 in the optimum efficiency case. Therefore, the inferred time constant is approximately equal to τ_{th}, with certainty for devices A–D.

4. Noise vs intermediate frequency

The output noise for each device was measured as a function of frequency in the case of optimum efficiency and in the overpumped case. The output noise was measured under identical conditions as for the measurements of the conversion efficiency. The results of these measurements of the output noise are plotted in Figs. 8 and 9. The points for frequencies above 1 GHz are averaged over a 500 MHz bin, and the points for frequencies below 1 GHz are averaged over a 100 MHz bin. A three-parameter fit to the equation

$$T_{\mathrm{out}}(\omega) = T_{\mathrm{John}} + \frac{T_{\mathrm{TF}}(0)}{1 + (\omega \tau_{\mathrm{eff}})^2} \tag{16}$$

was performed, varying $T_{\mathrm{TF}}(0)$, τ_{eff}, and T_{John}. Note that the 3 dB gain bandwidth (i.e., the frequency at which the conversion efficiency falls by a factor of 2) is predicted to be $(2\pi\tau_{\mathrm{eff}})^{-1}$, and the frequency at which the thermal fluctua-

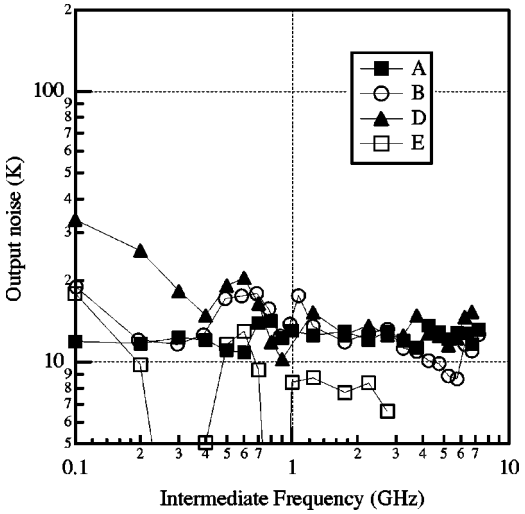

FIG. 9. Output noise vs intermediate frequency, overpumped case.

TABLE I. Device parameters and output noise; top half: optimum efficiency case; bottom half: overpumped case.

Dev.	L (μm)	$\eta(0)$ (dB)	$(2\pi\tau_{th})^{-1}$(GHz) from fit of η(f) to Eq. (2)	$(2\pi\tau_{th})^{-1}$(GHz) from fit of $T_{out}(f)$ to Eq. (16)	$T_{TF}(0)$(K) from fit of $T_{out}(f)$ to Eq. (16)	T_J(K) from fit of $T_{out}(f)$ to Eq. (16)	Noise BW (GHz)	$T_{mix}(0)\equiv T_{out}(0)/2\eta(0)$ (K,DSB)
A1	0.08	−5.6	⩾6	2.3	49	25	>6	120
A2	0.08	⋯	⩾6	⋯	⋯	⋯	⋯	⋯
B	0.16	−11	2.4	1.4	34	23	3.9	320
C[a]	0.24	−8	1.5	⋯	⋯	⋯	⋯	200
D	0.6	−4.1	0.3	0.13	262	19	0.73	120
E	3	−2[b]	0.08	0.13	223	8	0.75	530
A1	0.08	−7	⩾6	⩾6	⋯	⋯	>6	⩽100
B	0.16	−13.5	2.25	2.3	6	10	3.1	170
C	0.24	−12.7	1.5	⋯	⋯	⋯	⋯	160
D	0.6	−10.4	0.38	0.11	33	16	0.53	120
E	3	−11.7	0.064	0.045	62	7	0.16	310

[a]Device C was electrically damaged before the noise spectrum could be measured.
[b]The lowest efficiency measured was only −4 dB, but the fit returned a value of −2 dB because the lowest IF measured for this particular experiment was only 100 MHz.

tion noise component of the output noise falls by a factor of two is predicted to be the *same*, i.e., $(2\pi\tau_{eff})^{-1}$. Both quantities were varied in the fits to the measured conversion efficiency and output noise, in order to test this prediction experimentally.

The results of these fits are summarized in Table I. (The simultaneous measurements of noise and efficiency described in this section were performed with a slightly different experimental configuration than the measurements of efficiency alone described in the previous section. Hence the slight difference between the measured bandwidths for devices D and E between Table I and Fig. 7.) The relative spectrum of the output noise behaves similarly with frequency as the conversion efficiency, as can be seen by comparing the fitted time constant for the conversion efficiency and output noise. This implies that the 3 dB noise bandwidth is larger than the 3 dB gain bandwidth, which is also indicated by comparing the two quantities in Table I.

At high frequencies $[>(2\pi\tau_{th})^{-1}]$, the dominant noise source should be Johnson noise, with $T_J \approx 5.5$ K. Experimentally, we do not find this to be the case. (Device E was not well matched to the amplifier input impedance, so that the measured output noise at high frequencies was not expected to be equal to the electron temperature.) The excess we find for devices A, B, and D is approximately 13–19 K, larger than the maximum estimated uncertainty of ± 5 K. This may indicate an unidentified noise source. Further investigations will be necessary to elucidate this finding. Nonetheless, the data clearly demonstrate that there is a frequency scale associated with the dominant part of the output noise that scales with device length as it does for the gain bandwidth.

B. Device impedance measurements

The differential impedance of the device is an important quantity to know for circuit design purposes. In addition, measurements of the differential impedance can also test the underlying physical model. The simplest theoretical model available postulates that the differential impedance at frequencies well above τ_{th}^{-1} is simply V_{dc}/I_{dc}.[38] At high frequencies the electron temperature stays fixed. However, at frequencies below τ_{th}^{-1}, the electron temperature can follow the (slow) change in dissipated power, and the differential impedance is simply $(dV/dI)_{dc}$.

We used a directional coupler to measure the power reflected from the device in the intermediate state, i.e., the state when the electrons are at or near T_c due to the application of LO and dc power. (This was the state used for mixing measurements described above.) The device was biased in the superconducting state to provide a (scalar) calibration of the directional coupler and associated microwave components. The ''return loss'' is the power reflection coefficient in dB, i.e., $\mathrm{RL} \equiv -20\log(|\Gamma|)$, where Γ is the well known voltage reflection coefficient.

We found the return loss to be greater than 10 dB for all the devices measured, with the exception of device E, for frequencies both above and below τ_{th}^{-1}. These measurements are in agreement with the theoretical prediction.[39] The values of V_{dc}/I_{dc} and dV/dI fall within the range of 23–100 Ω, leading to a prediction of approximately 10 dB or greater for the return loss. Device E had values of V_{dc}/I_{dc} between 10 and 20 Ω, so that the return loss was between 3 and 7 dB, theoretically as well as experimentally. We also confirmed that the devices were well coupled in a broadband, resonance-free manner to the 50 Ω system in the normal state. This means that the mounting technique used provides a good 50 Ω transmission line system up to the terminals of the device, without any unwanted parasitic capacitance or inductance.

C. Normal state noise thermometry measurements

We used noise thermometry in the normal state where nonequilibrium superconducting effects are not important to demonstrate the crossover from diffusion to phonon cooling. The output noise and hence average electron temperature was measured as a function of applied dc power at a bath temperature above T_c, at 6 or 6.5 K, for several of the de-

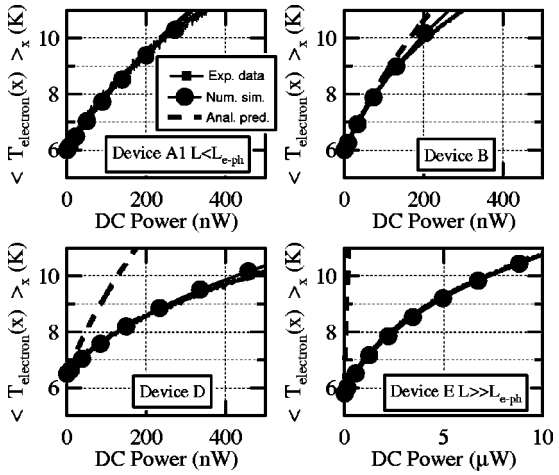

FIG. 10. Device temperature as a function of dc input power using noise thermometry. The numerical simulation includes both the electron–phonon interaction and diffusion cooling; the analytical prediction includes only diffusion cooling. Note the change in units on the abscissa for device E.

vices used in this work. The results of these measurements are plotted in Fig. 10. Since the length of device E is much longer than $L_{\mathrm{e-ph}}$, its temperature profile is uniform over most of the length of the bridge, except within $L_{\mathrm{e-ph}}$ of the ends. Plotting the increase in temperature with input power (as is shown in the last graph of Fig. 10) allows determination of the strength and temperature dependence of the electron–phonon interaction. The power law of the temperature dependence of the electron–phonon interaction for this device is well described by

$$p_{\mathrm{out}} = A(T_e^4 - T_{\mathrm{ph}}^4), \tag{17}$$

where p_{out} is the electron-phonon power flow per unit volume with $A = 2.34 \times 10^{10}\ \mathrm{W\,m^{-3}\,K^{-4}}$. This value is reasonably consistent with the value of $A = 0.98 \times 10^{10}\ \mathrm{W\,m^{-3}\,K^{-4}}$ found in Ref. 13 for samples of the same material, thickness, and diffusion constant. In the first graph in Fig. 10, the electron temperature versus input dc power is plotted for device A1, together with an analytical prediction[40,41] which neglects the electron–phonon interaction. Device A1 is sufficiently shorter than $L_{\mathrm{e-ph}}$ that the analytical solution describes the data very well.

A numerical solution to the diffusion equation was performed in Ref. 42 which included both heat diffusion and the electron–phonon interaction, with strength given by Eq. (17). The results of this simulation are plotted for all four curves in Fig. 10.[43] The simulation correctly describes the curves for devices B and D, for which both the electron–phonon interaction as well as diffusion contribute to cooling, as well as the devices at both limits, where only one or the other cooling mechanism dominates.

D. Comparison with theory

In this section, we compare the measured results of the coupled output noise and coupled conversion efficiency with the theoretical predictions presented in Sec. II. The predicted conversion efficiency and output noise based on Eqs. (3) and (12) was calculated for each device by using the maximum value of dR/dT measured with small bias current and no LO power. The value of dR/dT depends on the electron temperature, which may not be at the value which maximizes dR/dT when LO and dc power are applied. Since the predictions of the output noise and conversion efficiency increase monotonically with dR/dT, using the maximum possible value of dR/dT is expected to predict an upper limit for η and T_{TF}. A ''local'' value of dR/dT can be estimated by inferring the electron temperature from $R \equiv V_{\mathrm{dc}}/I_{\mathrm{dc}}$, and evaluating dR/dT at the inferred electron temperature from the measured R versus T curve. This method was carried out for the dc bias voltages which minimized the mixer noise in both the overpumped and optimum efficiency cases. The results of the calculated conversion efficiency based on this method are presented in Table II.

TABLE II. Predicted and experimental conversion efficiency and output noise; top half: optimum efficiency case; bottom half: overpumped case.

	$\eta(0)$ (dB)			$T_{\mathrm{out}}(0) = T_{\mathrm{TF}}(0) + T_J$ (K)[a]		
Dev.	Calc. from msd. R vs T max./local dR/dT used	Calc. using dR/dT from Eq. (18)	Expt.	Calc. from msd. R vs T max./local dR/dT used	Calc. using dR/dT from Eq. (18)	Expt.
A1[b]	+1.0/−5.3	−17.5	−5.6	237.5/60.5	9	37
B	+0.2/−3.2	−7	−11	389.5/180.5	78.5	51
C	+0.7/+0.2	−9.4	−8	671.5/223.5	20.5	44
D[c]	+0.3/-	−0.5	−5.4	365.5/-	179.5	118
E[c]	+0.3/-	0.0	−8.6	695.5/-	409.5	105
A1[b]	+2.3/0.0	−31	−7	165.5/91.5	5.6	14
B	−2.2/−4.0	−17.2	−13.5	115.5/78.5	9	14
C	+0.7/+0.2	−13.8	−12.7	330.5/145.5	7.8	17
D[c]	0.0/-	−8.8	−10.4	92.5/-	17.5	26
E[c]	−7.0/-	−3.7	−20	42.5/-	83.5	10

[a]A value of 5.5 K was assumed for T_J in the theoretical prediction.
[b]The output noise for device A quoted in this table was measured under slightly different operating conditions than that plotted in Fig. 1.
[c]The low frequency limit of the noise and efficiency is not well-determined for devices D and E, so the experimental value at 125–175 MHz is quoted in this table.

TABLE III. Comparison of JPL and Yale mixer results. The upper half of the table represents the results presented in this work measured at Yale, while the lower half represents the JPL data (Refs. 2–4,45–47).

Frequency (GHz)	Eff. (dB,SSB)	T_{out} (K)	T_{mix} (K,DSB)	T_{out} (K) (no LO pwr.)	L (μm)	R_N (Ω)	R_{sheet} (Ω)	Gain BW (GHz)
20[a]	−5.6	74	120	57	0.08	56	29	>6
20[a]	−11	57	320	⋯	0.16	80	29	2.4
20[a]	−8	44	200	30.6	0.24	96	29	1.5
533	−13.4±3[e]	41[b]	560[e]	36.7	0.27	20	10.4	1.7
1267	−13±3[e]	16.6[c]	450[e]	13.7	0.3	140	70	⋯
2500	−18.5±3[e]	10[d]	300[e]	<12	0.3	23	11.5	1.2

[a]Eff. referred to device. Bias conditions for optimum efficiency used. Output noise is extrapolated to $f=0$. Sheet resistance determined from larger device on wafer.
[b]Output noise is at 1.24–1.56 GHz.
[c]Output noise is at 1.24–1.56 GHz.
[d]Output noise is at 1.5 GHz. The 2.5 THz measurements were done at a bath temperature of 4.2 K, in contrast to the other data in the table where the bath temperature was approximately 2 K.
[e]The experimental technique used to determined $T_{mix}(0)$ in Refs. 2–4 was slightly different than that for this article. In all cases, however, the mixer noise is defined as $T_{out}/2\eta$; η is the intrinsic device conversion efficiency with no rf coupling circuit losses.

There is a separate way to determine the value of dR/dT, which uses the measured $I-V$curve. An increase in bias voltage increases the power dissipated, which raises the electron temperature. This in turn causes an increase in resistance. Based on this physical principle, a derivation is given in Ref. 31 for the following formula:

$$I_{dc}^2 dR/dP = I_{dc}^2 (dR/dT)/G = \frac{(dV/dI)-R}{(dV/dI)+R}. \tag{18}$$

The results of the calculated conversion efficiency based on this second method are also in Table II for all the devices.

For devices B and C the second method gives reasonable agreement between theory and experiment. Since the length of device A is comparable to the electron-electron length ($\sqrt{D\tau_{ee}}$, with τ_{ee}^{-1} the electron-electron scattering rate), a local equilibrium temperature cannot be well defined and the simple thermal model may not apply quantitatively to this device. We have also calculated the predicted output noise and conversion efficiency as a function of dc bias using method 2 [Eq. (18)] for all the devices studied in both the optimum efficiency and overpumped cases.[36] We find qualitative agreement between the theoretical and experimental dc bias dependence of the output noise and efficiency for all devices except device A. However, neither method provides consistent quantitative predictions of the magnitude of the conversion efficiency and output noise for a variety of operating conditions. A more microscopic approach which treats the spatial distribution of the superconducting energy gap in the presence of strong ac and dc self-heating, such as that being developed in Ref. 44, is desirable and may allow more quantitative predictions in the future. However, the simple thermodynamic model does correctly predict the frequency dependence of the conversion efficiency and output noise. Thus, absolute device performance cannot yet be quantitatively predicted from first principles and must continue to be investigated experimentally. Nevertheless, our experiments indicate that the device performance is excellent, i.e., the mixer noise is low.

V. COMPARISON TO OTHER WORK

In this section, we compare the results of experiments presented in this work (which were performed at Yale) with results on similar devices measured with 500 GHz,[2] 1.2 THz,[3] and 2.5 THz[45,4] signals (which were performed at JPL) in order to determine the relevance of the measurements presented in this work to actual THz receivers. A summary of the conversion efficiency and output noise measured at Yale and JPL is presented in Table III. The JPL measurements were generally tuned for lowest *receiver* noise by varying the applied dc and LO power. This condition depends on the details of the IF amplifier and rf coupling circuits, and is similar but not equivalent to both the optimum conversion efficiency and overpumped cases presented in this article. The devices used in Refs. 2–4 were approximately 0.3 μm in length, with sheet resistances between 10 and 70 Ω. In addition, the *unpumped* (no LO power applied) output noise of the devices measured for the present work, and those of Refs. 2–4, differed from one another, ranging from 57 to <12 K, indicating variation between the devices unrelated to the frequency of the applied LO and signal. Given these device-to-device variations, the measured mixer noise in all experiments is seen to be fairly consistent.

VI. CONCLUSION

We have shown the intermediate frequency dependence of the conversion efficiency and output noise of Nb hot-electron bolometers obey a simple thermal model. The thermal time constant for both the conversion efficiency and output noise is found to scale as L^{-2} for devices less than πL_{e-ph}, as expected for cooling by diffusion. The shortest device measured (L=0.08 μm) has a bandwidth larger than 6 GHz, the largest achieved for a low-T_c bolometer to date. We have also quantitatively demonstrated the crossover from diffusion to phonon-cooled behavior using noise thermometry in the normal state. The overall mixer noise is low,

100–500 K DSB, indicating that diffusion cooled bolometers are excellent candidates as mixers in THz receivers.

ACKNOWLEDGMENTS

We thank A. Kozhevnikov for assistance with the experiments, and P. Chalsani for simulations of the temperature profiles. This research was supported by the NSF and by the NASA Office of Space Science. Funding for PJB was provided by a NASA Graduate Student Fellowship as well as a Connecticut High Technology Fellowship.

[1] J. Kawamura, R. Blundell, C. Y. Tong, G. Gol'tsman, E. Gershenzon, and B. Voronov, Appl. Phys. Lett. **70**, 1619 (1997).
[2] A. Skalare, W. R. McGrath, B. Bumble, H. G. LeDuc, P. J. Burke, A. A. Verheijen, R. J. Schoelkopf, and D. E. Prober, Appl. Phys. Lett. **68**, 1558 (1996).
[3] A. Skalare, W. McGrath, B. Bumble, and H. G. LeDuc, IEEE Trans. Appl. Supercond. **7**, 3568 (1997).
[4] B. S. Karasik, M. C. Gaidis, W. R. McGrath, B. Bumble, and H. G. LeDuc, Appl. Phys. Lett. **71**, 1567 (1997).
[5] R. Blundell and C. E. Tong, Proc. IEEE **80**, 1702 (1992), special issue on THz technology.
[6] M. J. Wengler, Proc. IEEE **80**, 1810 (1992), special issue on THz technology.
[7] E. Gershenzon, M. Gershenzon, G. Gol'tsman, A. Semenov, and A. Sergeev, J. Exp. Theor. Phys. Lett. **34**, 268 (1981).
[8] E. Gershenzon, M. Gershenzon, G. Gol'tsman, A. Semenov, and A. Sergeev, J. Exp. Theor. Phys. Lett. **36**, 269 (1982).
[9] E. Gershenzon, M. Gershenzon, G. Gol'tsman, A. D. Semenov, and A. Sergeev, J. Exp. Theor. Phys. **59**, 442 (1984).
[10] E. Gershenzon, M. Gershenzon, G. Gol'tsman, A. Semyonov, and A. Sergeev, Solid State Commun. **50**, 207 (1984).
[11] E. Gershenzon, G. N. Gol'tsman, A. Elant'ev, B. Karasik, and S. E. Potoskuev, Sov. J. Low Temp. Phys. **14**, 414 (1988).
[12] E. Gershenzon, M. Gershenzon, G. Gol'tsman, A. M. Lyul'kin, A. Semenov, and A. Sergeev, Sov. Phys. Tech. Phys. **34**, 195 (1989).
[13] E. Gershenzon, M. Gershenzon, G. Gol'tsman, A. M. Lyul'kin, A. Semenov, and A. Sergeev, J. Exp. Theor. Phys. **70**, 505 (1990).
[14] E. Gershenzon, G. Gol'tsman, I. G. Gogidze, Y. P. Gusev, A. I. Elant'ev, B. S. Karasik, and A. Semenov, Superconductivity **3**, 1582 (1990).
[15] G. Gol'tsman, A. Semenov, Y. P. Gousev, M. A. Zorin, I. G. Gogidze, E. Gershenzon, P. T. Lang, W. J. Knott, and K. F. Renk, Supercond. Sci. Technol. **4**, 453 (1991).
[16] Y. P. Gousev, G. Gol'tsman, A. Semenov, E. Gershenzon, R. Nebosis, M. Heusinger, and K. Renk, J. Appl. Phys. **75**, 3695 (1994).
[17] A. Dzardanov, H. Ekström, G. Gol'tsman, S. Jacobsson, B. Karasik, E. Kollberg, O. Okunev, and S. Yngvesson, in *Proceedings of the International Conference on Millimeter and Submillimeter Waves and Applications*, edited by M. N. Afsar (SPIE, San Diego, 1994), pp. 276–278, sponsored by the SPIE.
[18] G. N. Gol'tsman, B. S. Karasik, O. V. Okunev, A. L. Dzardanov, E. M. Gershenzon, H. Ekström, S. Jacobsson, and E. Kollberg, IEEE Trans. Appl. Supercond. **5**, 3065 (1995).
[19] B. S. Karasik, G. N. Gol'tsman, B. M. Voronov, S. I. Svechnikov, E. M. Gershenzon, H. Ekström, S. Jacobsson, E. Kollberg, and K. S. Yngvesson, IEEE Trans. Appl. Supercond. **5**, 2232 (1995).
[20] H. Ekström, B. Karasik, E. Kollberg, G. Gol'tsman, and E. Gershenzon, in *Proceedings of the 6th Internation Symposium on Space Terahertz Technology*, edited by J. Zmuidzinas and G. Rebiez (CalTech, Pasadena, CA, 1995), pp. 269–283. See Ref. 48.
[21] P. Yagoubov, G. Gol'tsman, B. Voronov, L. Seidman, V. Siomash, S. Cherednichenko, and E. Gershenzon, in *Proceedings of the 7th International Symposium on Space Terahertz Technology*, edited by R. M. Weikle, G. M. Rebeiz, and T. W. Crowe (University of Virginia, Charlottesville, VA, 1996), pp. 290–302. See Ref. 49.
[22] J. Kawamura, R. Blundell, C. Y. Tong, G. Gol'tsman, E. Gershenzon, and B. Voronov, J. Appl. Phys. **80**, 4232 (1996).
[23] P. Yagoubov, G. Gol'tsman, B. Voronov, S. Svechnikov, S. Cherednichenko, E. Gershenzon, V. Belitsky, H. Ekström, E. Kollberg, A. Semenov, Y. Gousev, and K. Renk, in *Proceedings of the 7th International Symposium on Space Terahertz Technology*, edited by R. M. Weikle, G. M. Rebeiz, and T. W. Crowe (University of Virginia, Charlottesville, VA, 1996), pp. 303–317. See Ref. 49.
[24] S. Cherednichenko, P. Yagoubov, K. Il'in, G. Gol'tsman, and E. Gershenzon, in *Proceedings of the 8th International Symposium on Space Terahertz Technology*, edited by R. Blundell and E. Tong (Harvard–Smithsonian Center for Astrophysics, Cambridge, Massachusetts, 1997), pp. 245–257.
[25] D. E. Prober, Appl. Phys. Lett. **62**, 2119 (1993).
[26] D. W. Floet, J. R. Gao, W. Hulshoff, H. van der Stadt, T. M. Klapwijk, and A. K. Suurling, Inst. Phys. Conf. Ser. **158**, 401 (1997).
[27] K. Fiegle, D. Diehl, and K. Jacobs, IEEE Trans. Appl. Supercond. **7**, 3552 (1997).
[28] P. J. Burke, R. J. Schoelkopf, D. E. Prober, A. Skalare, W. R. McGrath, B. Bumble, and H. G. LeDuc, Appl. Phys. Lett. **68**, 3344 (1996).
[29] P. J. Burke, R. J. Schoelkopf, D. E. Prober, A. Skalare, B. S. Karasik, M. C. Gaidis, W. R. McGrath, B. Bumble, and H. G. LeDuc, Appl. Phys. Lett. **72**, 1516 (1998).
[30] F. Arams, C. Allen, B. Peyton, and E. Sard, Proc. IEEE **54**, 612 (1966).
[31] H. Ekström, B. Karasik, E. Kollberg, and K. Yngvesson, IEEE Trans. Microwave Theory Tech. **43**, 938 (1995).
[32] B. Karasik and A. Elantev, in *Proceedings of the 6th Internation Symposium on Space Terahertz Technology*, edited by J. Zmuidzinas and G. Rebiez (CalTech, Pasadena, CA, 1995), pp. 229–246. See Ref. 48.
[33] B. S. Karasik and A. I. Elantiev, Appl. Phys. Lett. **68**, 853 (1996).
[34] J. C. Mather, Appl. Opt. **21**, 1125 (1982).
[35] The case of a lumped element connected to a bath *through* a distributed system was considered in Refs. 32–34.
[36] P. J. Burke, Ph.D. thesis, Yale University, 1997, available from authors.
[37] B. Bumble and H. G. LeDuc, IEEE Trans. Appl. Supercond. **7**, 3560 (1997).
[38] A. Elant'ev and B. Karasik, Sov. J. Low. Temp. Phys. **15**, 379 (1989).
[39] In this section, we neglect the difference between τ_{th} and $\tau_{th}/(1-\alpha_0)$; the latter is the correct quantity to use for the crossover frequency of the device impedance (Refs. 32 and 33).
[40] C. Smith and N. Wybourne, Solid State Commun. **57**, 411 (1986).
[41] M. J. M. de Jong, Ph.D. thesis, Leiden University, 1995.
[42] P. Chalsani, Simulations of the Temperature Profile in a Hot Electron Bolometer, 1997, senior Thesis, Yale University.
[43] The Lorenz number was varied in Ref. 42 for the simulations and analytical solutions plotted in Fig. 10 in order to obtain the agreement shown. The free electron value is $\mathcal{L}=2.45\times10^{-8}\,\mathrm{W\,\Omega\,K^{-2}}$; this was adjusted to $3.3\times10^{-8}\,\mathrm{W\,\Omega\,K^{-2}}$, which is acceptable since experimentally determined values of $\mathcal{L}$ generally depend on temperature and material.
[44] D. W. Floet, J. Baselmans, J. Gao, and T. Klapwijk, in *Proceedings of the 9th International Symposium on Space Terahertz Technology*, edited by W. McGrath (Caltech, Pasadena, CA, 1998).
[45] B. Karasik, M. Gaidis, W. McGrath, B. Bumble, and H. G. LeDuc, IEEE Trans. Appl. Supercond. **7**, 3580 (1997).
[46] A. Skalare (unpublished).
[47] B. Karasik (unpublished).
[48] In *Proceedings of the 6th Internation Symposium on Space Terahertz Technology*, edited by J. Zmuidzinas and G. Rebiez (CalTech, Pasadena, CA, 1995).
[49] In *Proceedings of the 7th International Symposium on Space Terahertz Technology*, edited by R. M. Weikle, G. M. Rebeiz, and T. W. Crowe (University of Virginia, Charlottesville, VA, 1996).